Hindawi
Advances in Materials Science and Engineering
Volume 2018, Article ID 7259424, 16 pages
https://doi.org/10.1155/2018/7259424

Research Article

Finite Element Modeling of FRP-Strengthened RC Beam under Sustained Load

Shiyong Jiang, Weilai Yao, Jin Chen, and Tao Cai

Department of Military Infrastructure Engineering, Army Logistics University of PLA, Chongqing, China

Correspondence should be addressed to Shiyong Jiang; jiangshiy@163.com

Received 21 April 2018; Accepted 14 September 2018; Published 1 November 2018

Academic Editor: Antonio Boccaccio

External bonding of FRP laminates to the tension soffit of concrete members has become a popular method for flexural strengthening. However, the long-term field performance of FRP-strengthened RC members under service conditions is still a concern, and more work needs to be done. Based on concrete smeared-crack approach, this paper presents a finite-element (FE) model for predicting long-term behavior of FRP-strengthened RC beam, which considers the time-dependent properties of all components including the aging effect of concrete. According to the comparison between theoretical predictions and test results, the validity of the FE model is verified. The interfacial edge stresses in adhesive layer were determined through appropriate mesh refinement near the plate end, and their time-dependent characteristics were investigated. The results show that creep of concrete and epoxy resin cause significant variations of the edge stresses with time. According to the research in this paper, the FE approach is found to be able to properly simulate the long-term behavior of the FRP-strengthened beam and help us better understand the complex changes in the stress state occurring over time.

1. Introduction

Using fiber-reinforced polymer (FRP) composites as externally bonded reinforcement is in the forefront of retrofitting technology. Most of previous studies have been rightfully focused on the ultimate limit state behavior [1–3]. Relatively few studies have been performed on the behavior of FRP-strengthened RC structures under long-term services conditions. In fact, under sustained load, concrete exhibits clear creep response, and the viscous property of adhesive is remarkable [4–7]. Related to the kind of fiber used and fiber content, some types of FRP products may also present noticeable viscoelasticity [8–10]. As time goes on, structure deformation increases and cracks further develop, which negatively affects the serviceability [11]. In addition, it has been shown that the creep deformation of very old concrete can still be substantial [12, 13]. Thus, if a structure is strengthened because the service load will be increased, although the concrete may be aged, creep response caused by the additional load should still receive critical attention. Nevertheless, the long-term response of strengthened members is not fully explored, and further research is essential in order to enhance the safety and design of FRP-strengthened members [14, 15].

So far, previous studies have proposed some analytical methods to investigate time-dependent characteristic of RC structure strengthened by external reinforcement [11, 16–19]. It can be found that most of them are based on cross section analyses, which satisfy strain compatibility and equilibrium of forces. One of the drawbacks of the analytical method is that it may be difficult to consider some significant characteristics. For instance, the basic mechanism for strengthening is the shear deformation and stress transferring of epoxy adhesive between concrete and external FRP. Normally, epoxy presents evident flow property [20, 21], which therefore leads to relaxation of interfacial stress and affects the long-term behavior. Whereas, it is actually not easy to model such shear creep characteristic of adhesive in cross section analyses. Besides, the tension stiffening of concrete needs to be reasonably taken into account when predicting deflections. Nevertheless, for the method of section analysis, it is also a challenging task to

model such tension-stiffening effect appropriately and accurately. Thus, it can be noted that the above influential factors are usually roughly approximated and even neglected [11, 16, 19]. On the other hand, in order to improve the efficiency of solving process or reduce the difficulty in mathematics, simplifications have been ordinarily introduced in analytical method. Based on axial strain reduction coefficient and curvature reduction coefficient, Hong and Park [11] calculated the time-dependent change of the concrete stress in a simple and empirical way. Marí et al. [16] assumed that the stresses of tension bars and FRP laminate remain constant over time. Although, reasonable theoretical results are still obtained in their studies [11, 16], there is no evidence to show those simplifications are suitable for other cases, where the creep responses of materials, the geometry of member, and reinforcement ratio (for steel and FRP) are different. It is therefore implied that the universality of the analytical method applying specific simplification is not favorable enough. Additionally, it should be noted that despite simplifications have been made, large amount of iterative calculations still may be needed to obtain the final results [11]. Moreover, the stresses at the adhesive interfaces near the bonding edges are responsible for the debonding failures, and their redistribution with time is an issue worth studying. Nevertheless, when determining and investigating the time-dependent interfacial stresses, cross section analyzing is no longer competent, and a quite different analysis procedure (particularly to interfacial forces) needs to be carried out [22, 23]. In the related studies, it can be found that although precise and complicated derivations had been conducted, assumption not fully corresponding to the fact was still made in order to make the mathematical process more manageable [22, 23]. The stresses within the adhesive layer were assumed to be constant through the thickness of the adhesive layer in both studies of Benyoucef et al. [22] and Zhang and Wang [23], which in fact vary strongly across the layer thickness [24].

To eliminate the aforementioned deficiencies, finite element (FE) modeling may be a feasible scheme. Comparing to the analytical method, to study the behavior of FRP-strengthened RC member under sustained load, the FE method may provide a more powerful tool, which calculates numerically and does not operate on the basis of cross section analysis. Those specific simplifications mentioned above may also be avoided, which makes the FE method more generally applicable. However, to date, studying the time-dependent performance by FE approach has not been extensively conducted. One of the likely reasons should be that reasonably developing time-dependent constitutive models of materials can be a challenging task.

The major thrust of this paper is to propose a finite element model to investigate the long-term response of FRP-strengthened RC beam under sustained load. The time-dependent characteristics of all components including the evolution of concrete property along with time were modeled as user-defined subroutines in ABAQUS 6.12 [25]. Besides, load sustaining experiment of a strengthened beam was also conducted. By comparing the experiment and FE results, the validity of the FE model is demonstrated. Also, interfacial stresses were accurately determined by the same FE model, with appropriate mesh refinement near the end of CFRP plate. Additional numerical investigations were carried out to study the changes of edge stresses over time induced by the creep of materials.

2. Long-Term Deformation Monitoring

Time-dependent deformation of a FRP-strengthened RC beam under sustained load was monitored for 200 d. The sectional dimension was 250 × 400 mm with a 30 mm thickness. The total and effective span was 3300 mm and 2900 mm, respectively. D28 reinforcement (diameter is 28 mm) was used for reinforcement on the compression side, while D14 reinforcement (diameter is 14 mm) was used for reinforcement on the tension side. Under service state, concrete stress is not high, which presents linear creep. In this study, adequate compression bars were used to control instantaneous stress in compressive concrete at lower level simulating the service condition. CFRP plate with length and width of 2600 and 200 mm was bonded on the tension soffit of beam. D8 (diameter is 8 mm) reinforcement at interval of 200 mm was used for the stirrups. To avoid premature debonding near the end of CFRP plate, CFRP sheets were used to wrap around the test beam. Figure 1 provides the detailed information of the test beam.

The test beam was cast by commercial concrete. The 28-day cylinder compressive strength of the concrete was 34.0 MPa. Other parameters of concrete are listed in Table 1. Table 2 shows the properties of steel reinforcement. Table 3 gives the properties of epoxy resin (applied as adhesive), CFRP sheet (for avoiding premature debonding), and CFRP plate (for flexural strengthening). The reported material strengths above are measured mean values.

The test beam was simply supported and loaded in four point bending. The sustained load F was 75% of the theoretical ultimate capacity F_u (on the basis of cross section analysis) of the same dimensional RC beam without strengthening. The beam was cured for 7 d, then placed indoors for another 69 d before loading. In the test, a dedicated experimental system, made up of vertical reaction frame, screw jack, and steel distribution beam, was designed to apply and sustain the external load, as illustrated in Figure 2. Load was applied to the beam through slowly lifting up the screw jack, meanwhile, its value was monitored by the force sensor at the top of the jack. As the value reached to 0.75 F_u (117.71 kN), screw jack was locked to prevent lifting or declining, which sustained the load. When the deformation of test beam increased due to creep behavior, the applied load might decrease, then the Jack was unlocked and further lifted up to replenish the force to the designed level (0.75F_u). During the long-term test, the error of applied load was controlled within ±1% of the planned value.

As shown in Figure 1, in the midspan, resistance strain gauges were bonded to the tension, compression steel, and CFRP plate to measure the instantaneous strains only, since their long-term working performance is unreliable. Vibrating wire gauges were especially used to obtain both

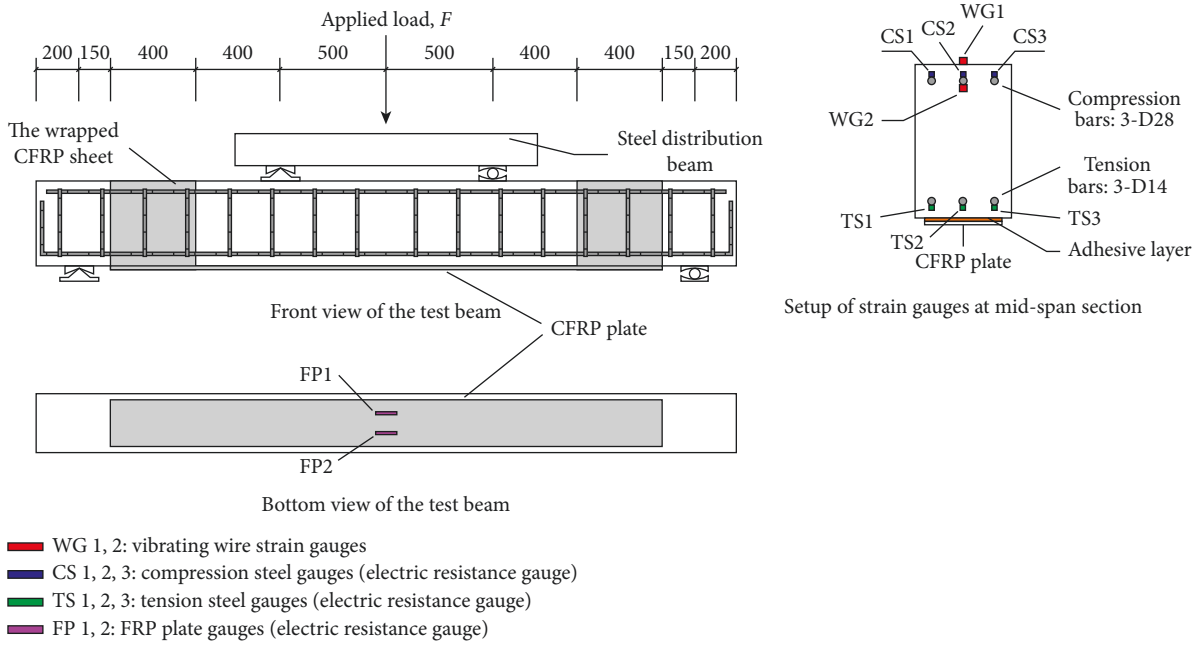

Figure 1: Test beam details.

Table 1: Concrete properties.

Slump of fresh concrete (mm)	Ratio of fine aggregate to total aggregate by weight (%)	Cement content (kg/m^3)	Fly ash content (kg/m^3)	Water cement ratio
220	38	325	60	0.4

Table 2: Materials' properties of steel reinforcement.

Reinforcement type	Yield strength (MPa)	Ultimate strength (MPa)
Tension, D14	461	625
Compression, D28	420	570
Shear, D8	435	610

Table 3: Adhesive and CFRP properties.

	Ultimate strength in tension (MPa)	Elastic modulus (GPa)	Thickness (mm)
Epoxy resin layer	39.6	3.468	1.4
CFRP sheet	3510	241	0.15
CFRP plate	2482	174	1.4

instantaneous and long-term strains in some places because of their reliable performance in long period of monitoring. The 1# wire strain gauge (WG1) was bonded on the top surface of the beam. The 2# wire strain gauge (WG2) tied with the middle compression bar was buried in the specimen when casting concrete. One dial gauge was installed at the bottom midspan point and other two dial gauges installed at pedestals were used mainly to check the symmetrical nature of the loaded beam.

The experiment was conducted indoors. Figure 3 shows the recorded temperature and humidity, which presented unavoidable variations with time. It should be noted that the observed creep might be affected by the change of environmental conditions in the laboratory.

3. FE Modeling

Based on ABAQUS 6.12 [25], nonlinear numerical analysis was performed to study the time-dependent characteristics of concrete beam strengthened with external FRP reinforcement. The FE model used herein is on the basis of the one developed by Jiang et al. [26]; however, the current FE model in this paper was further updated and is more advanced: the aging effect of concrete was taken into account and the corresponding calculating method was presented, and also, the method for analyzing the time-dependent interfacial stress was developed.

3.1. Modeling of Instantaneous Material Property. In this study, concrete cracking was simulated by using the smeared-cracked approach. Unlike the discrete-crack approach, there is no need to predefine the crack paths in the smeared-cracked approach. In addition, aiming to overcome the mesh-nonobjectivity problem in the conventional smeared-crack approach, the crack band model was used [27].

The concrete was modeled within the framework of the concrete-damaged plasticity model provided by

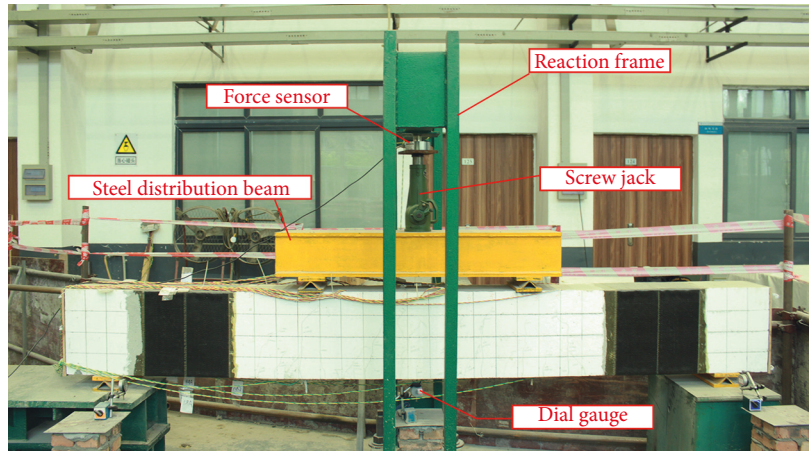

Figure 2: Experiment setup in laboratory.

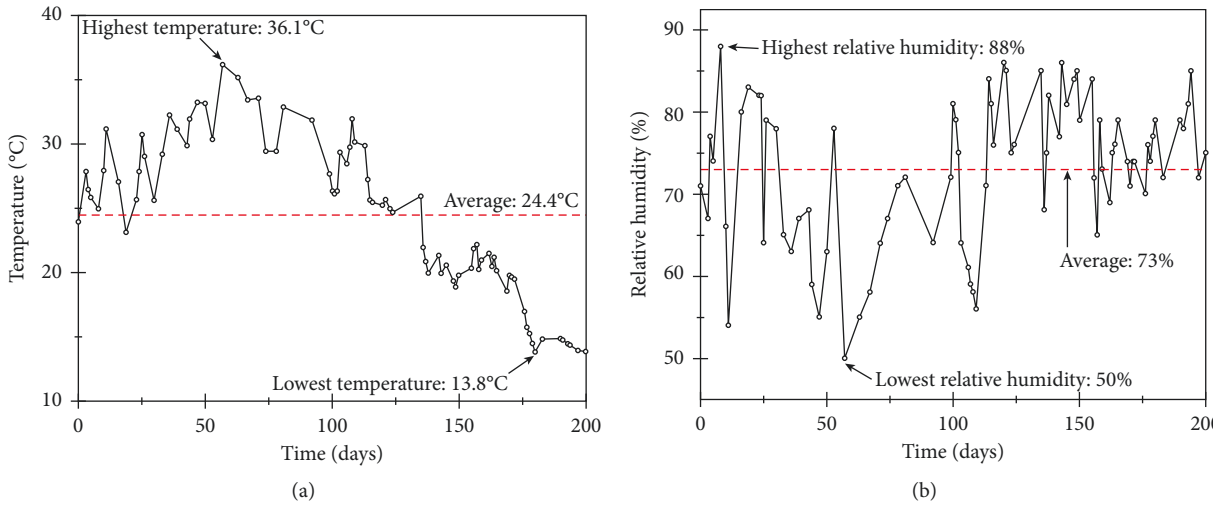

Figure 3: Environmental conditions during test. (a) Temperature indoors. (b) Relative humidity indoors.

ABAQUS. The stress-strain relationship under uniaxial compression recommended by Saenz [28] (Equation (1)) was applied. Under uniaxial tension, the problem involves tensile cracking. The stress-crack opening displacement curve recommended by Hordijk [29] (Equations (2) and (3)) was used. The parameters in Equations (2) and (3) can be further determined through Equations (4) and (5) based on CEB-FIP standard [30]. Figure 4 presents the uniaxial mechanical behavior of concrete.

$$\sigma_c = \frac{E_0\varepsilon_c}{1+\left(\left(\left(E_0\varepsilon_{cp}\right)/f_c\right)-2\right)\left(\varepsilon_c/\varepsilon_{cp}\right)+\left(\varepsilon_c/\varepsilon_{cp}\right)^2}, \quad (1)$$

$$\frac{\sigma_t}{f_t} = \left[1+\left(c_1\frac{w_t}{w_{cr}}\right)^3\right]e^{\left(-c_2\left(w_t/w_{cr}\right)\right)} - \frac{w_t}{w_{cr}}\left(1+c_1^3\right)e^{\left(-c_2\right)}, \quad (2)$$

$$w_{cr} = 5.14\frac{G_F}{f_t}, \quad (3)$$

$$f_t = 1.4\left(\frac{f_c-8}{10}\right)^{2/3}, \quad (4)$$

$$G_F = \left(0.0469d_a^2 - 0.5d_a + 26\right)\left(\frac{f_c'}{10}\right)^{0.7}, \quad (5)$$

where σ_c and σ_t (in MPa) are the compressive and tensile stress, respectively. The f_c and f_t are the uniaxial compressive and tensile strength, respectively. The ε_c is the compressive strain; ε_{cp} is the peak compressive strain (0.002) corresponding to the strength f_c; E_0 is the elastic modulus, according to ACI 318 [31], $E_0 = 4730\sqrt{f_c}$ (in MPa). The w_t (in mm) is the crack opening displacement; w_{cr} (in mm) is the crack opening displacement at the complete release of stress and fracture energy; $c_1 = 3.0$ and $c_2 = 6.93$ are constants determined by test; G_F is the energy required to create a unit area of stress-free crack; d_a (in mm) is size of the maximum aggregate and is assumed as 20 mm if no experimental data are available.

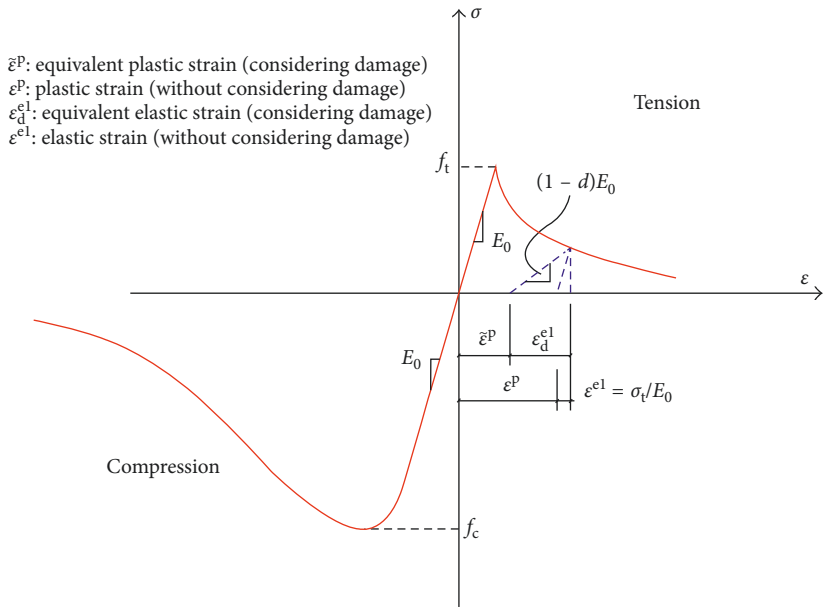

Figure 4: Uniaxial mechanical behavior of concrete and the damage pattern.

Based on Bazant and Planas [32], mesh sensitivity problem can be effectively overcome through applying the crack band model [33], in which the displacement of crack opening w equals to the cracking strain ε_{cr} accumulating over the width of the crack band h_c.

$$w = \int_{h_c} \varepsilon_{cr}\, dh. \tag{6}$$

According to Rots [34], when meshing concrete with four-node plane stress element with four integration points, the crack band width is taken to be $\sqrt{2}e$, where e is the side length of the element [27]. Thus, the tensile stress-crack opening displacement relationship given by Equation (2) can be transformed into a stress-strain curve needed by FE program through Equation (6).

The damage evolution was also considered to better describe the nonlinearity of concrete. The relationship between the damage factor d and plastic strain ε^{p}, which does not take stiffness degradation into account was defined. Damage factor can be determined as Equation (7) according to Tao and Chen [35] for both uniaxial tension and compression. The patterns of damage are illustrated in Figure 4.

$$d = \frac{(1 - \sigma/f)\varepsilon^{p}}{(1 - \sigma/f)\varepsilon^{p} + \sigma/E_0}, \tag{7}$$

where σ is the uniaxial tensile or compressive stress and f is uniaxial tensile or compressive strength.

In this study, the response of FRP-strengthened RC beam under service state is investigated, therefore, the instantaneous material properties of epoxy adhesive, steel reinforcements, and CFRP plate were modeled as linear elastic. Also, perfect bonds were assumed between adhesive-concrete, adhesive-CFRP plate, and concrete-steel. The wrapped CFRP sheets for avoiding premature debonding were reasonably ignored in the FE model based on the relatively low stress level [20].

3.2. Modeling of Time-Dependent Material Property. Under sustained load, concrete presents significant creep behavior, and additional stress-independent shrinkage deformation is also considerable. The different time-dependent characteristics of materials induce complicated stress redistribution in structure along with time.

The loading age is written as t_0, and the load sustaining period is from t_0 to t_n $(t_n > t_0)$. The total time period t_0 to t_n is divided by a number of discrete periods: t_0 to t_1, t_1 to t_2,. . ., t_{n-2} to t_{n-1}, t_{n-1} to t_n. This paper presents a quasielastic constitutive model of concrete considering creep and shrinkage based on age-adjusted effective modulus method (Equations (8)–(10)). The model is in recursion form, which comforts codes programming and improves calculating efficiency. The detailed derivation process of Equations (8)–(10) can be found in Jiang et al. [26], which is not presented herein for brevity.

$$\sigma^{*}(t_n) = \frac{E(t_{n-1})}{1 + \chi(t_n, t_{n-1})\left[\sum_{j=1}^{m} b_j(t_{n-1})\left[1 - e^{-\lambda_j \cdot \Delta t_n}\right]\right]} \cdot (\varepsilon_n - \Delta\varepsilon), \tag{8}$$

$$\Delta\varepsilon = \varepsilon_{sh}(t_n) - \varepsilon_{sh}(t_{n-1}) + \sum_{j=1}^{m} A_{n,j}^{*} \cdot \left(1 - e^{-\lambda_j \cdot \Delta t_n}\right), \tag{9}$$

$$A_{n,j}^{*} = A_{n-1,j}^{*} \cdot e^{-\lambda_j \cdot \Delta t_{n-1}} + b_j(t_{n-2}) \cdot e^{-\lambda_j \cdot \Delta t_{n-1}} \cdot \frac{\chi(t_n, t_{n-2})}{E(t_{n-2})} \cdot \sigma^{*}(t_{n-1}) \quad \text{for } n > 1. \tag{10}$$

When $n = 1$:

$$A^{*}_{n=1,j} = b_j(t_0) \cdot \frac{\sigma_0}{E(t_0)}, \tag{11}$$

where $\sigma^{*}(t_i)$ is the stress increment of concrete due to the effect of creep and shrinkage from t_{i-1} to t_i, reflecting the redistribution of stress within structure; $E(t_i)$ is the elastic modulus at time t_i; $\varepsilon_{sh}(t_i)$ refers to the shrinkage strain at time t_i; and $\Delta t_i = t_i - t_{i-1}$ $(i = 0, 1, 2, \ldots, n-1, n)$. The b_j, λ_j, and m are material parameters for expanding the creep coefficient $\varphi(t, \tau)$ as Dirichlet series [26] (Equation (12)). The $\chi(t_n, t_{n-1})$ is the aging coefficient [36] (Equation (13)). The σ_0 refers to the instantaneous stress state under loading. The ε_n is the strain increment of concrete during t_{n-1} to t_n, which reasonably considers the effects of stress increment induced by creep and shrinkage.

$$\varphi(t, \tau) = \sum_{j=1}^{m} b_j(\tau)\left[1 - e^{-\lambda_j (t-\tau)}\right], \tag{12}$$

$$\chi(t, \tau) = \frac{1}{1 - e^{-\varphi(t,\tau)}} - \frac{1}{\varphi(t, \tau)}. \tag{13}$$

Due to the progress of hydration, concrete properties including strength and elastic modulus develop with time. The above time-dependent elastic modulus of concrete $E(t_i)(i = 0, 1, 2, \ldots, n-2, n-1, n)$ was determined by the time-dependent concrete strength $f_c(t_i)$ (concrete strength at time t_i) according to ACI 318 [31] ($E_c = 4730\sqrt{f_c}$). The time interval (t_0 to t_1, t_1 to t_2, …, t_i to t_{i+1}, …, t_{n-2} to t_{n-1}) was set small (less than 5 d) to obtain accurate enough result. The elastic modulus of concrete was assumed to be constant in each time interval, but renewed and updated when calculation of the latest time interval was finished. In this way, the aging effect of concrete was considered. This study applied the evolution law of concrete strength proposed by ACI 209 [37].

$$f_c(t_i) = f_{c28} \cdot \left(\frac{t_i}{a + b \cdot t_i}\right), \tag{14}$$

where f_{c28} is the concrete mean compressive strength at 28 d in MPa and t_i is the age of concrete in days. $a = 4.0$ and $b = 0.85$ are material constant for concrete using ordinary Portland cement. In this study, the test beam was loaded at the age of 76 d after casting concrete. Thus, the calculated 76 d strength 37.7 MPa and its corresponding elastic modulus 29.0 GPa were used to determine the instantaneous response of the test beam under loading. The evolution of concrete property along with time is shown in Figure 5.

The above time-dependent property of concrete was programmed as FORTRAN code in user-defined subroutine UEXPAN and USFLD in ABAQUS. Concrete creep coefficient and shrinkage strain was calculated using ACI 209 code [37], and during the calculation, the measured average humidity (73%) was used.

In this study, both shear and axial creep of adhesive resin were modeled in the FE approach. For FRP-strengthened system, the performance of adhesive is of crucial importance in providing effective stress transfer. It has been demonstrated

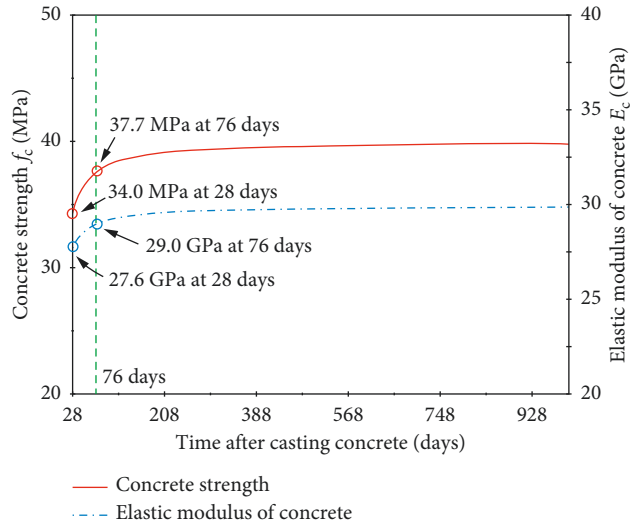

Figure 5: The evolution of concrete property with time.

that epoxy adhesive presented evident viscoelastic manner [20, 21, 38]. As a result, the relaxation of interfacial stresses caused by adhesive creep affects the strengthening mechanism, which therefore influences the long-term response of strengthened beam. In this research, to describe the decreased shear relaxation modulus of epoxy $G_a(t)$ with time, Maxwell chain was used [20, 21].

$$G_a(t) = G_u + \sum_{i=1}^{N_G} G_i \cdot e^{-t/\tau_{Gi}}, \tag{15}$$

where G_u is the shear modulus at infinite time, N_G is number of Maxwell elements, G_i refers to the relaxed shear modulus of the ith Maxwell element, and τ_{Gi} is material constant. Following Choi [20], $N_G = 1$, $\tau_{G1} = 2$ d, and $G_u = G_1/5$. In addition, the creep of epoxy in axial direction was also taken into account, since near the midspan, where section moment is large and the instantaneous stress of epoxy resin in axial direction usually reaches a noticeable value, which causes nonignorable creep response. It is assumed that Poisson's ratio of adhesive ν_a remains constant with time [39, 40], and so, the relaxation modulus in axial direction $E_a(t)$ is derived from that in the shear direction or vice versa: $E_a(t) = 2(1 + \nu_a)G_a(t)$ [14, 15].

The viscous property of CFRP was determined as follows [41]:

$$\varepsilon_{CFRP}(t) = \varepsilon_0 \cdot \sinh\left(\frac{\sigma}{\sigma_m}\right) + m \cdot \sinh\left(\frac{\sigma}{\sigma_m}\right) \cdot t^{n_1}, \tag{16}$$

where $\varepsilon_{CFRP}(t)$ = time-dependent strain; t = time after loading, in hour; and σ = applied stress. The $\varepsilon_0 = 0.379$; $\sigma_m = 68950$ MPa; $m = 0.0011$; $n_1 = 0.123$ are material constants [41]. Similar to concrete, the above mechanical properties of adhesive and CFRP related to time were also programmed in user subroutines UEXPAN and USFLD.

3.3. Solution Strategy. In the FE model, only a half of the beam was included by taking advantage of symmetry about

midspan plane, which effectively reduces calculating time. The concrete, epoxy adhesive, and CFRP plate were modeled by plane stress element CPS4. The steel reinforcement was modeled using truss elements.

During the FE analyses, step-by-step procedures were applied for calculations. Instantaneous behavior of the beam was calculated first, which was set as the initial condition of the calculation of long-term response afterwards. Then, based on the time-dependent properties of materials, numerical simulation of long-term behavior of the test beam was carried out. In this study, if not otherwise stated, square element with an element size of 10 mm was used to model concrete. Matching element sizes were chosen to represent the steel bars, the epoxy layer, and the FRP plate. The epoxy layer and the FRP plate were each modeled with two layers of elements in their thicknesses. Nevertheless, when discussing the time-dependent interfacial stresses at the bonding edge, mesh refinement is needed, which is particularly mentioned in the later section.

4. Results and Discussion

4.1. Verification of the Recommended FE Model. Under instantaneous loading, comparison of FE-predicted results and experimental results of the specimen is shown in Table 4. As shown in Figure 1, the tension steel gauge, compression steel gauge, and FRP plate gauge are labeled as TS, CS, and FP. Several strain gauges were employed at the place of midspan: TS1, TS2, and TS3 were bonded to each of the tension bar; CS1, CS2, and CS3 were bonded to each of the compression bar; and FP1 and FP2 were adjacently bonded to the CFRP plate. In Table 4, the strain of tension bar, compression bar, and CFRP plate is the average value of the measured data by TS1, TS2, TS3; CS1, CS2, CS3; FP1, and FP2, respectively. The strain of the top concrete of test beam was obtained by the 1# wire strain gauge (WG1). Table 4 shows that the test results are reasonably predicted by the FE model.

From Table 4, the compressive strain of top concrete is 277 $\mu\varepsilon$ under instantaneous loading, indicating the stress level does not exceed 40 percent of strength, thus, applying the linear creep theory for concrete is appropriate in this paper. The time-dependent midspan deflection is shown in Figure 6(a). The time-dependent strains of top concrete and the concrete near compression bars are presented in Figure 6(b), which were experimentally obtained by the vibrating wire gauges WG1 and WG2, respectively. Distinct additional long-term deformation was observed during load sustaining period. After time passage of 200 d, the deflection, strain of top concrete, and strain of concrete near compression bars were respectively 56.7%, 98.6%, and 59.2% higher than their initial value under instantaneous loading. The increasing of deformation corresponds to the typical law of RC member under sustained load: quick in early period and slow in later time. From Figure 6(a), it is shown that after sustaining load for 78 d (39% of the total time period), most part of additional long-term deflection (87.2%) is finished. Also, as shown in Figure 6(b), there are no clear increases for the strains of concrete after 78 d of sustaining load. The results (FE1) predicted by the FE model agree well with the experimental results. The predicted time-dependent deflection at the 50, 99, 155, and 200 d after sustaining load is 4.97, 5.24, 5.42, and 5.52 mm, respectively, which is close to the corresponding test values of 5.00, 5.43, 5.52, and 5.59 mm, with differences of only 0.6%, 3.5%, 1.8%, and 1.3%, respectively. The time-dependent strains of top concrete, concrete near compression bars, are also predicted with good accuracy as shown in Figure 6(b). Besides, The predicted results (FE2) without considering the further evolution of concrete property are also displayed in Figure 6. As expected, neglecting the evolution of concrete property leads to overestimated results, however, with slight effect only. The reason is that the maturity of the used commercial concrete has been good enough after 76 d of aging (the time that the long-term test commenced), as shown in Figure 5.

The result of FE1 and FE2, respectively, refers to the case with and without considering the evolution of concrete property. The additional deflection (Δf) is defined as the delayed deflection occurring in load sustaining period. The total additional deflection (Δf_{total}) is the delayed deflection after 200 d of sustaining load. The ration between Δf and Δf_{total} represents the creep progress of the test beam.

As shown in Figure 6, in this study, the test results of both strain and deflection do not present continuing growth along with time, which is likely to be caused by the fluctuations of environmental humidity and temperature [11]. However, effects of climate changing were currently not considered during FE modeling; therefore, the predicted long-term deformation increases continuously and smoothly. Whereas, from the comparison above, the accuracies of the FE results are favorable enough.

The proposed FE model rationally predicts the cracking behavior of concrete. Figure 7(a) shows the experimentally observed cracking pattern of test beam under instantaneous loading. In this study, because adequate stirrups were deployed to prevent the occurrence of shear failure, in the earlier stage of loading, the observed cracks were flexural cracks in vertical direction mainly. With the increasing of load, new cracks gradually emerged in the bending-shear section, propagating vertically first but then obliquely afterwards. As shown in Figure 8, the FE results appropriately simulate this phenomenon. The effect of tension stiffening, which causes the concrete between adjacent cracks to suffer tensile stress, is also simulated by the FE model, as presented in Figure 8(c). During the test, further development of instantaneous cracks during load sustaining period was clearly observed (Figure 7(b)). The combined effect of materials' creep behaviors and decreasing of section stiffness induced by further formation of cracks causes the additional long-term deformation of test beam.

The instantaneous cracks are marked by color grey; the further development of cracks in long-term are marked by color red.

The FE model in this paper has been further validated against the test results in other literatures [42, 43]. Totally, seven specimens are selected herein: four of them are from Sobuz et al. [42] including one control beam (not strengthened) and three CFRP-strengthened beams and the other three are from Tan and Saha [43]. Sobuz et al. [42]

Table 4: Immediate response at midspan of the test beam.

Results	Deflection (mm)	Strain of tension steel bar ($\mu\varepsilon$)	Strain of compression steel bar ($\mu\varepsilon$)	Strain of CFRP plate ($\mu\varepsilon$)	Strain of top concrete ($\mu\varepsilon$)
Test	3.57	878	−129	937	−277
FE model	3.68	785	−137	845	−248
Theor./exp.	1.03	0.89	1.06	0.90	0.89

Note. Theor./exp. in the above table refers to the ratio of result predicted by FE model and test result, which reflects the predicting error.

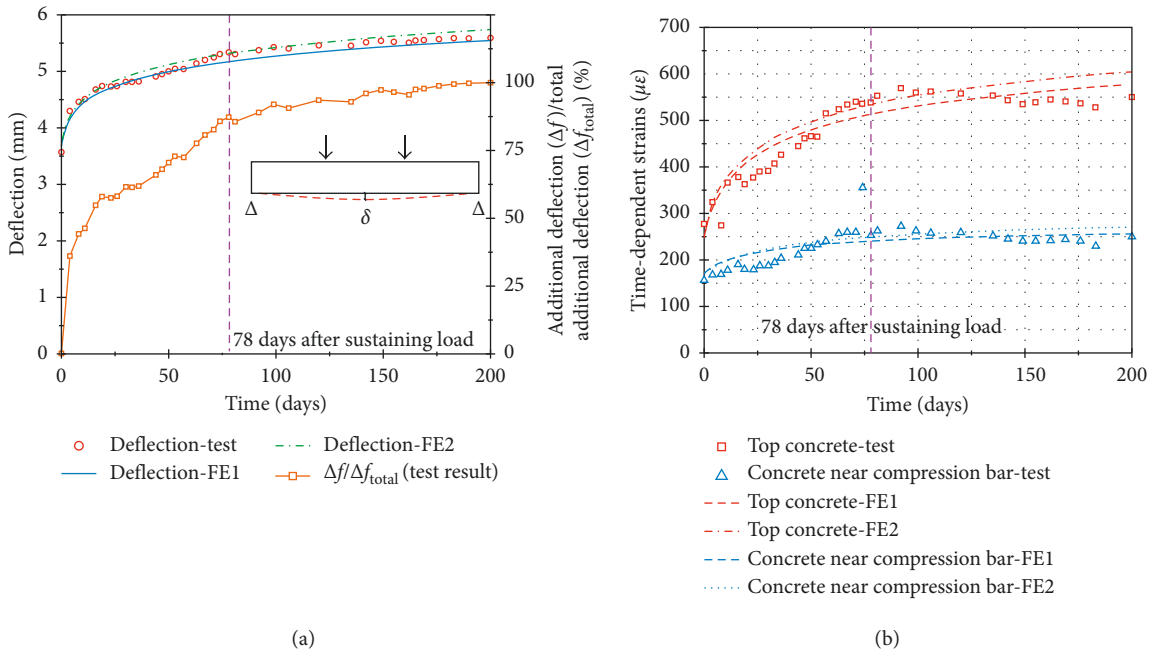

Figure 6: Test and FE results of the specimen. (a) Deflection at the midspan. (b) Concrete strains.

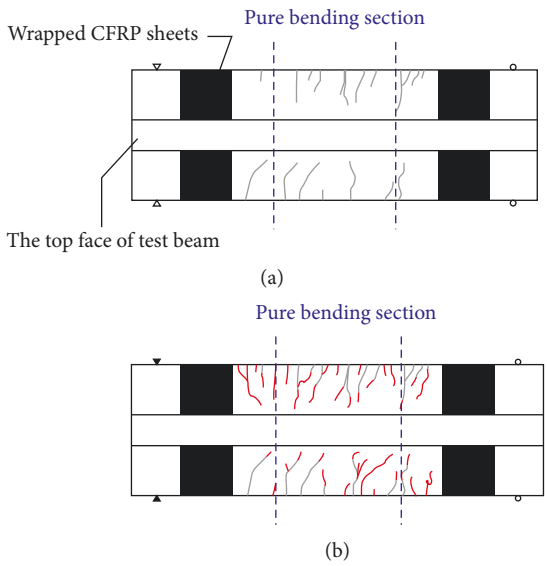

Figure 7: Cracking pattern observed experimentally (unfolded-drawing). (a) At instantaneous loading. (b) After time passage (200 d).

studied the effects of strengthening scheme and level of sustained load on long-term response of RC beam strengthened by CFRP. Four representative specimens are selected herein to demonstrate the accuracy of the proposed FE approach, namely, CBC (not strengthened, the control beam), FBC-1L, FBC-2L, and FBC-3L. Tan and Saha [43] tested the time-dependent responses of nine GFRP-strengthened specimens. Three typical specimens are chosen herein, namely, GB3-40, GB3-49, and GB3-59. Table 5 presents the detailed information of these specimens.

According to Sobuz et al. [42] and Tan and Saha [43], the viscoelasticity of FRP plate was ignored. The aging effect of concrete was considered based on the aforementioned method in Section 3.2. For the specimens from Sobuz's test [42], the ultimate creep coefficient and ultimate shrinkage strain of concrete were 1.87 and 418 $\mu\varepsilon$, which were determined through *3.2.1.1 Compressive creep test* and *3.2.1.2 Drying shrinkage test* in Sobuz's paper [42]. For the specimens from Tan's study [43], the specific laws of concrete creep and shrinkage have been given in their paper [43], which were, therefore, directly used in the FE simulations. From Figure 9, the proposed FE approach well predicts the test results.

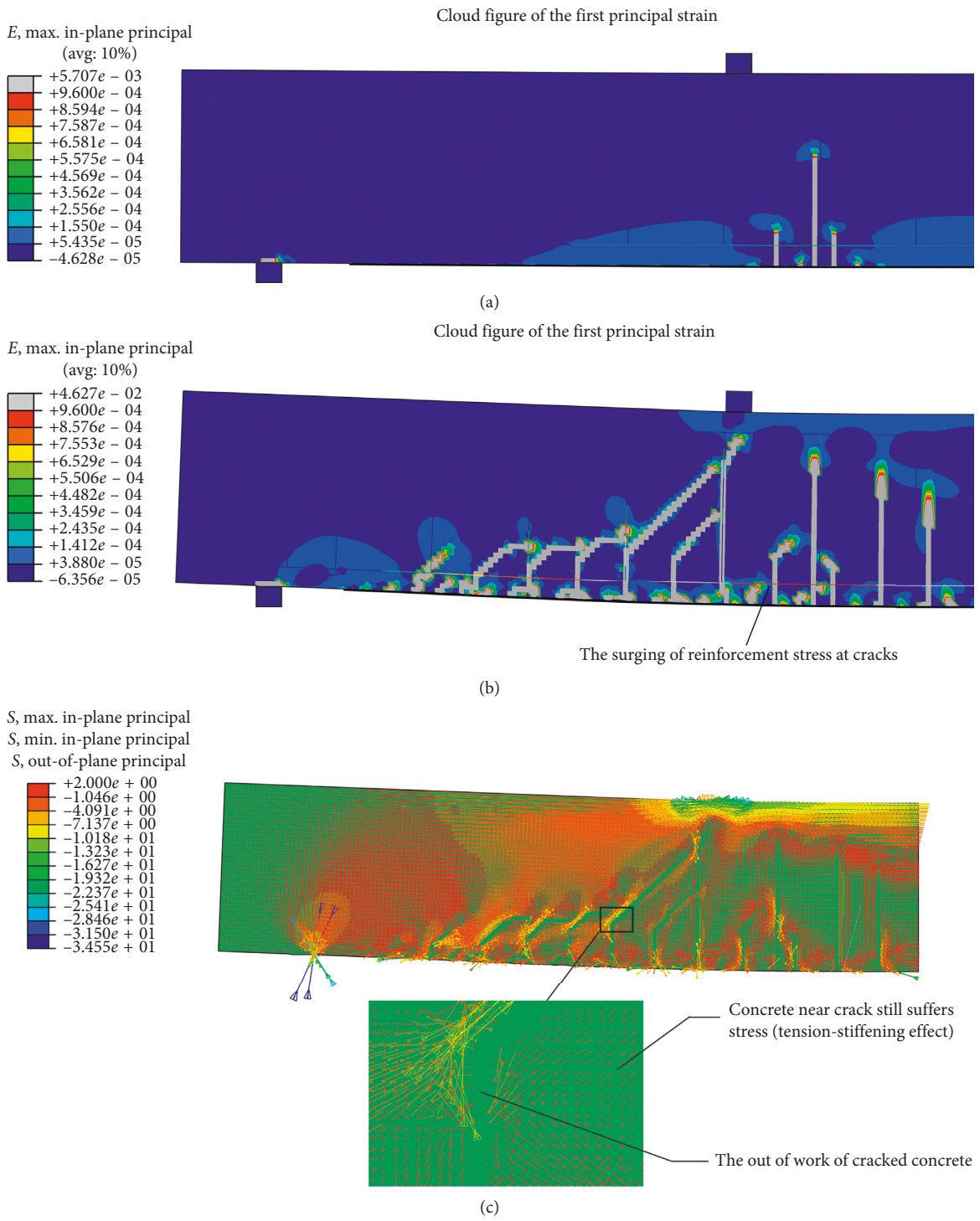

Figure 8: FE cracking pattern. (a) Cracking pattern as 50% of instantaneous load applied. (b) Cracking pattern as 100% of instantaneous load applied. (c) Principle stress presented by vector field (MPa).

4.2. Time-Dependent Interfacial Edge Stresses. The bonding interfaces are critical regions that transfer stresses between concrete and FRP. One of the most concerned issues of RC beams reinforced by FRP is the premature debonding at the plate edges or near cracks, where the stresses (both shear and vertical normal) in the adhesive layer are relatively high. In this paper, numerical investigations were performed to study the time-dependent edge stresses of adhesive interface through the proposed FE approach. The FE model was established on the basis of the test beam in the experimental study of this paper. The responses of specimen under different levels of applied load F (23.54 kN, 47.08 kN, and 70.62 kN) were simulated. Since the wrapped CFRP sheets near the end of beam were not modeled, their

Table 5: Properties of selected specimens for numerical simulation.

Source		Sobuz et al. [42]				Tan and Saha [43]		
Beam name		CBC	FBC-1L	FBC-2L	FBC-3L	GB3-40	GB3-49	GB3-59
Beam dimensions	Span L (mm)	1900				1800		
	Height h_c/width b_c (mm)	200/150				125/100		
Concrete	28-day cylinder compressive strength f_c (MPa)	36.0				30.4		
	Modulus of elasticity E_c (GPa)	28.6				27.2		
Steel	Tension reinforcement area (mm^2)/yield strength f_{yt} (MPa)/elastic modulus E_{st} (GPa)	157/482/195				157/520/194		
	Compression reinforcement area (mm^2)/yield strength f_{yc} (MPa)/elastic modulus E_{sc} (GPa)	57/470/186				57/525/183		
FRP reinforcement	Nominal thickness (n × ply thickness t_r)/width b_{frp} (mm)	—	1.2 × 1/100	1.2 × 2/100	1.2 × 3/100	0.8 × 3/100		
	Ultimate strength f_r (MPa)/elastic modulus E_r (GPa)	—	1685/165			1700/39		
Applied moment at midspan (kN·m)		7.144				4.740	5.640	6.840

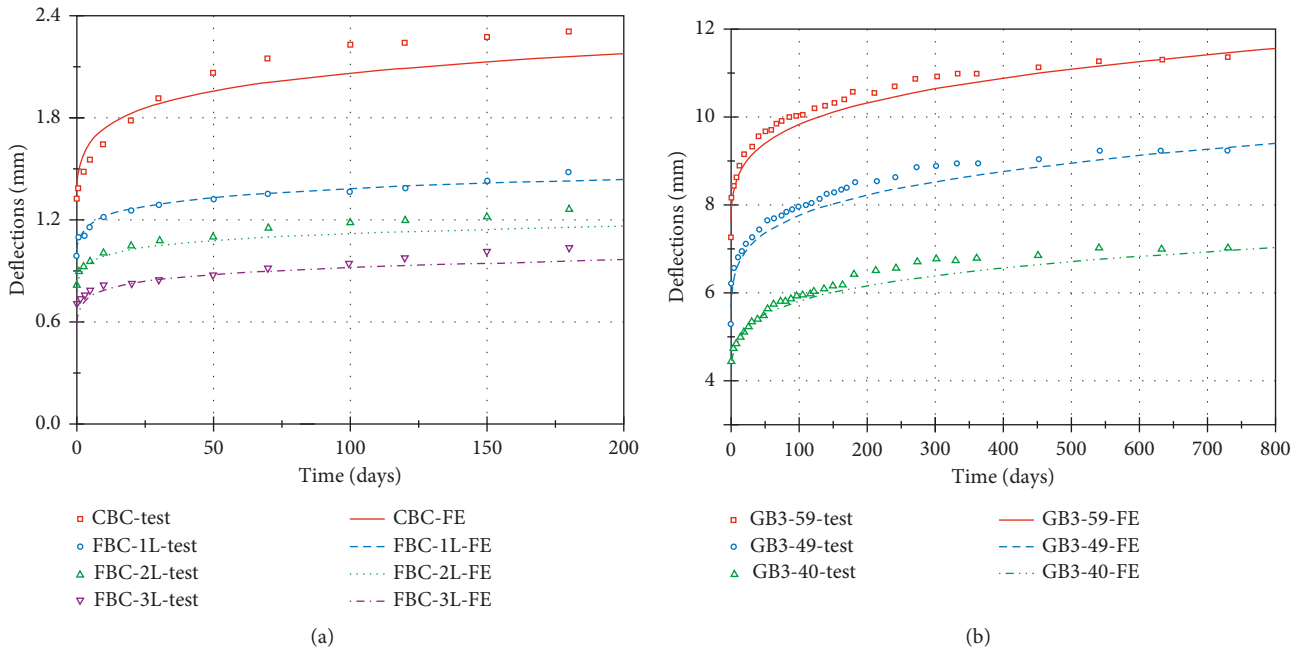

Figure 9: FE versus test deflections at midspan. (a) FE and test results for Sobuz's [42] specimens. (b) FE and test results for Tan's [43] specimens.

influences on the localized interfacial stresses were not discussed currently.

As shown in Figure 10, due to the existence of singular points (Point A and B), in order to obtain accurate stresses, the region near the plate end needs a particularly fine mesh. Following the recommendation of Teng et al. [24], in the vertical direction, for the adhesive layer, the top part (near concrete-adhesive interface) and the bottom part (near adhesive-FRP plate interface) were, respectively, meshed by two layers of elements (the height of each element is 0.1 mm). The rest part of the adhesive layer was evenly meshed by other three layers of elements. In the horizontal direction, a graded mesh was used starting with an aspect ratio of 1 for the minimum height (0.1 mm) elements. The CFRP plate has the same mesh pattern as the adhesive layer. A graded and matching mesh was adopted for the concrete. The stress distribution near the plate end under instantaneous loading is given in Figures 11 and 12 (applied load F = 70.62 kN), whose characteristics correspond to the findings of previous researches [24, 44]. It shows that high vertical normal (peeling) and shear stresses exist near the bonding end, which are responsible for the debonding failures widely reported in tests. Also, the normal and shear stresses vary strongly across the thickness of the adhesive layer in the vicinity of the end of the plate. This aspect cannot be captured by existing approximate analytical solutions [22, 23] developed with the assumption that stresses are invariant across the adhesive thickness.

AC interface refers to adhesive-to-concrete interface, PA interface refers to plate-to-adhesive interface, and MA refers

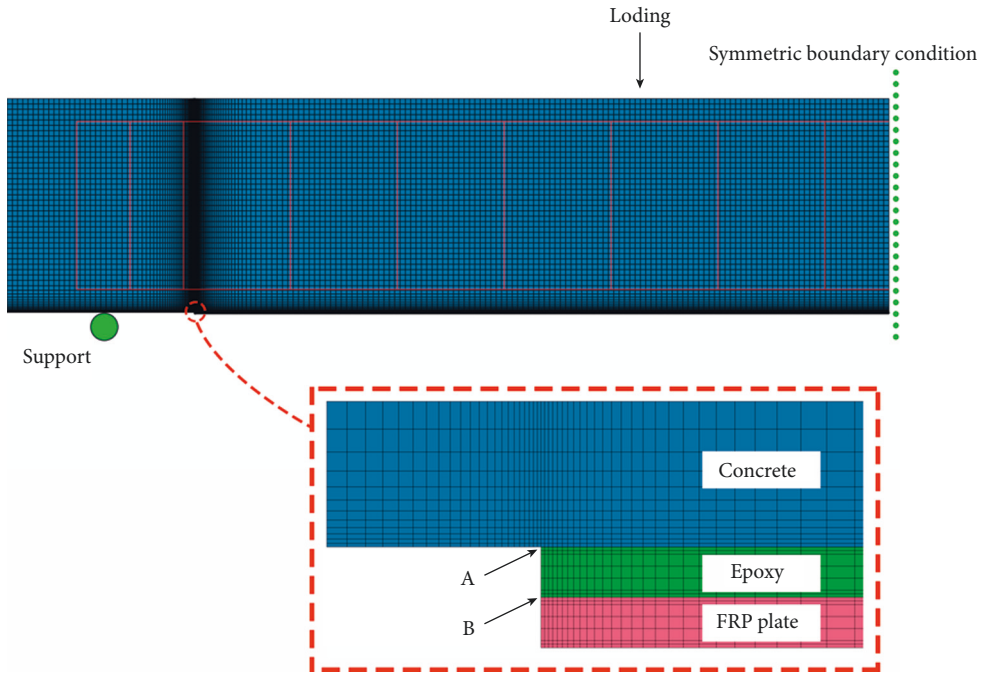

Figure 10: The element refinement near the plate end.

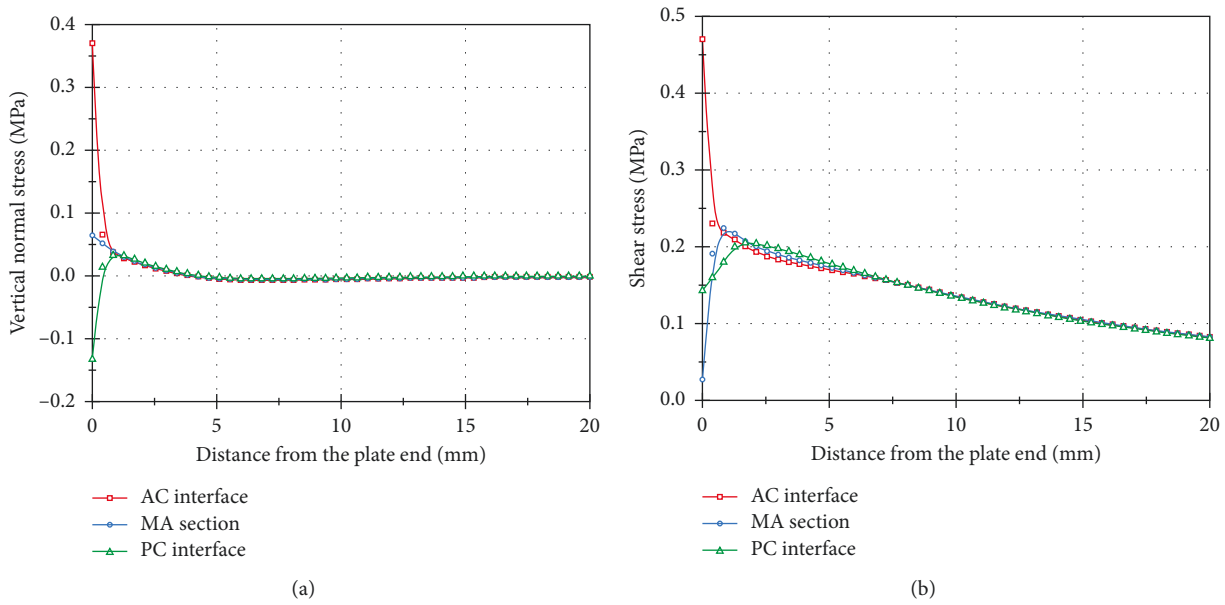

Figure 11: Interfacial Stress distributions under instantaneous loading. (a) Vertical normal stress. (b) Shear stress.

to the horizontal section of the adhesive layer obtained by a horizontal cut at midthickness.

In this research, the time-dependent characteristic of interfacial edge stress at point A (in AC interface) is especially discussed, which is one of the most important factors causing debonding failures. The changes of interfacial shear and vertical normal stresses with time are shown in Figure 13. In this case, only the creep of adhesive in shear direction is considered (both FRP and concrete are modeled as time-invariant materials). Figures 13(a) and 13(b) show the viscous flow of epoxy in shear direction leading to significant relaxations for both shear and vertical normal stresses at the plate end. With the increase of sustained load, the level of instantaneous stress in epoxy layer is promoted, which causes more evident creep response and stress relaxation. In Figure 13, the relaxation rate of stress is fast in the earlier stage, but almost slows down to zero afterwards. Such phenomenon is believed to be induced by the shear creep law of adhesive adopted herein, which presents that most of creep deformation develops within relatively short time period compared to the well-known long creep period of concrete [21]. For the results shown in Figure 14, the axial

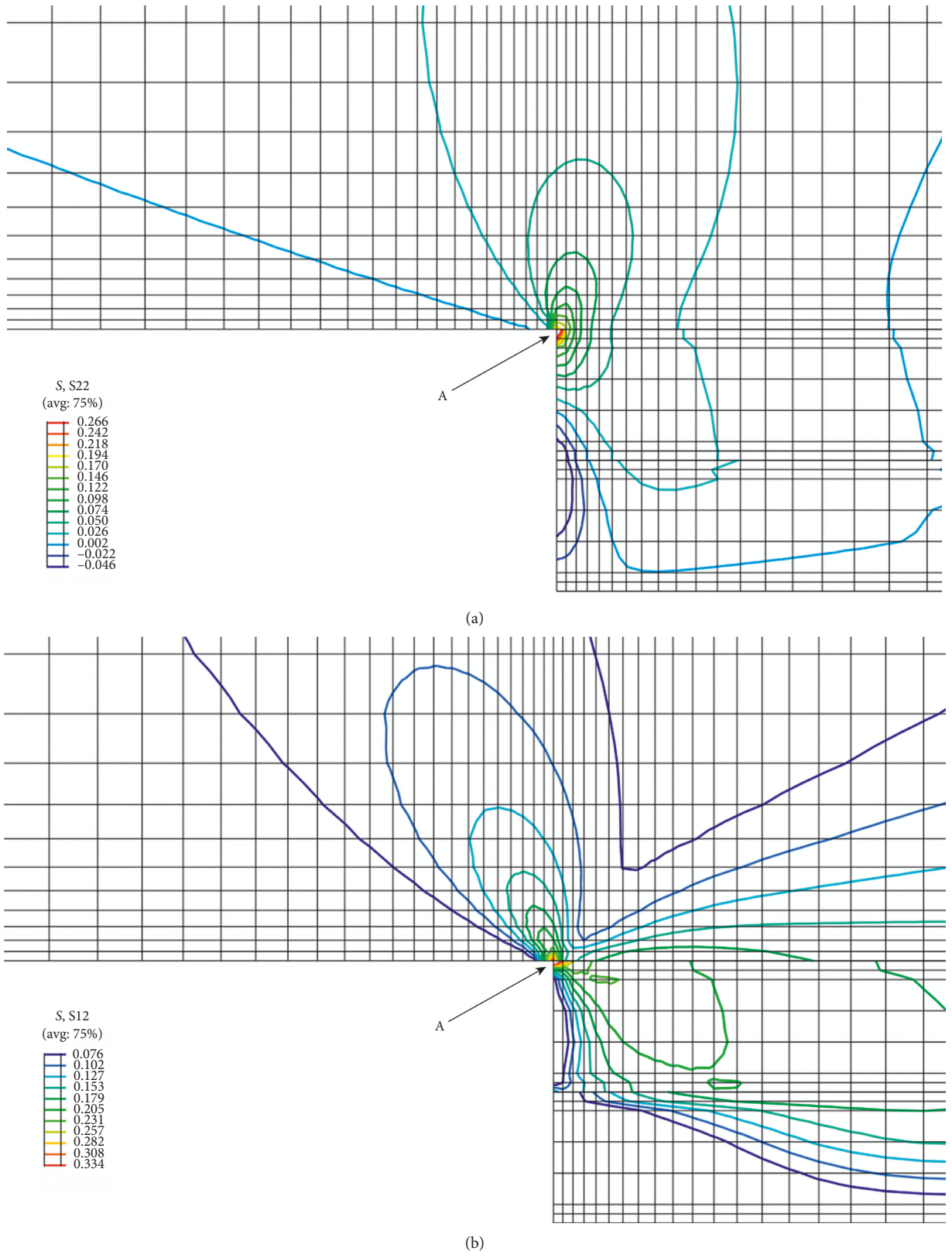

Figure 12: Contours of stress near the plate end (MPa). (a) Vertical normal stress. (b) Shear stress.

creep of epoxy is only considered to separately investigate its effect on the edge stress. It is shown that like the shear creep, the axial creep of adhesive also causes relaxations of the edge stresses, however, with a much more inferior effect. The likely reason is that near the plate end, the section moment is small, and there is low axial stress in the adhesive layer;

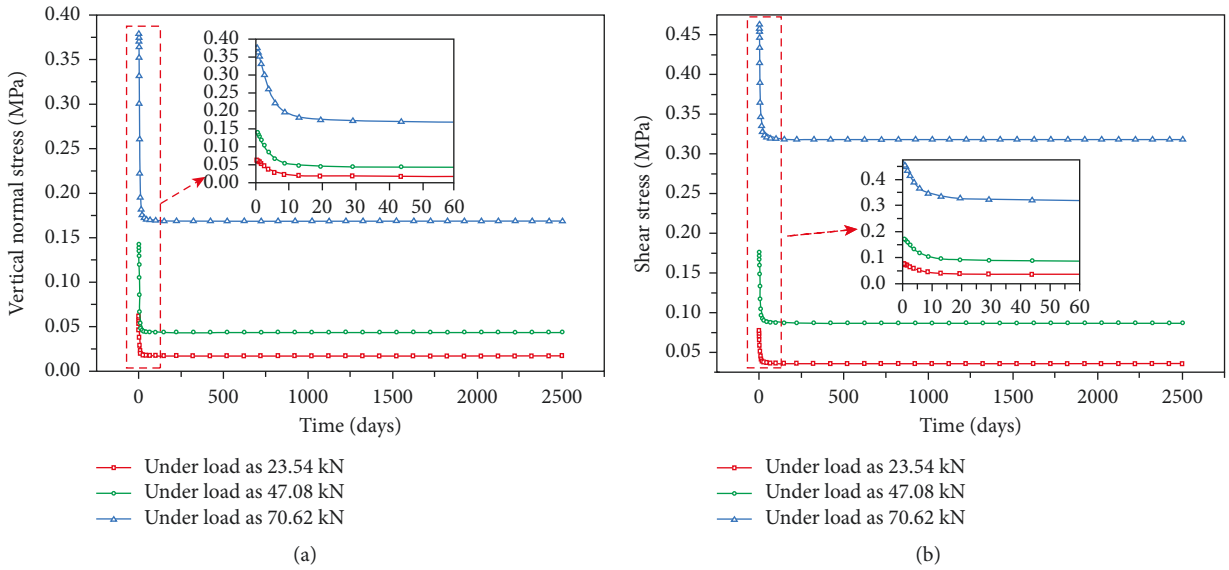

FIGURE 13: The separate effect of shear creep of adhesive on the edge stresses. (a) Variation of vertical normal stress with time. (b) Variation of shear stress with time.

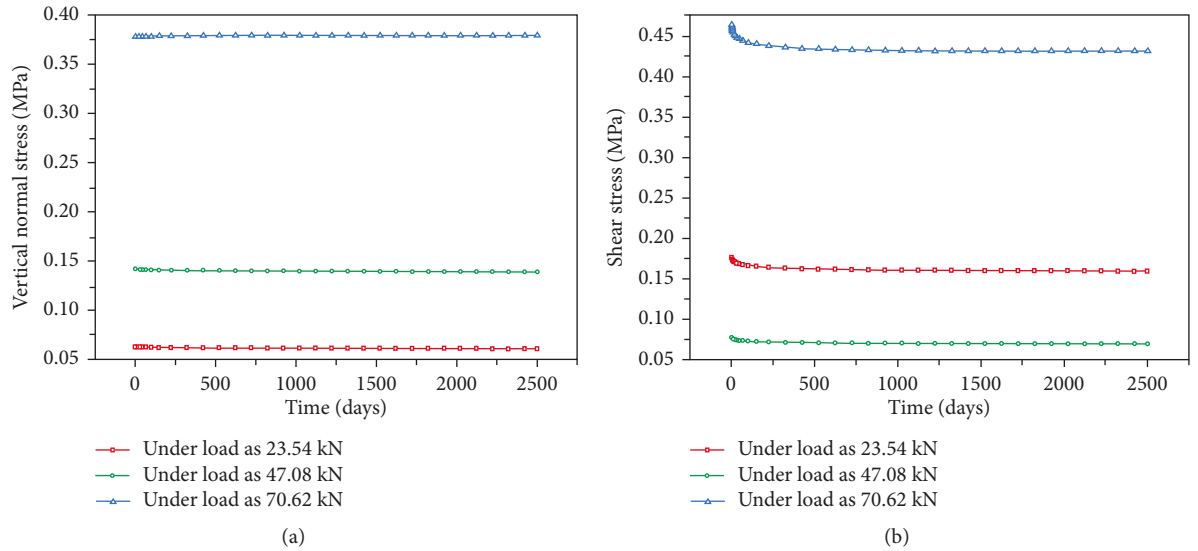

FIGURE 14: The separate effect of axial creep of adhesive on the edge stresses. (a) Variation of vertical normal stress with time. (b) Variation of shear stress with time.

hence, the axial creep is not obvious, which does not clearly influence the edge stresses.

The combined effect of concrete creep and adhesive creep was also investigated, as illustrated in Figure 15. It is found that the creep of concrete individually leads to increases of both interfacial shear and vertical normal stresses along with time, which may eventually lead to premature debonding. This corresponds to the findings in previous studies [14, 15, 45], which demonstrates the rationality of the suggested FE approach. However, as the creep of concrete and adhesive occurs at the same time, the relaxation effect by adhesive creep counteracts the increasing effect by concrete creep on the edge stresses to some extent. Therefore, the edge stresses present lower increases with time, comparing to the case that concrete creep works separately. As the relaxation effect is evident enough, which is larger than the increasing effect of concrete creep, the stresses even show decreases in the earlier stage (curve A, B, and C in Figure 15). Following that, the creep of adhesive is almost completed, while the creep of concrete is still significant; thus, there is an ongoing increase for the edge stresses afterwards. Besides, since the relaxation effect of adhesive creep in axial direction is smaller, its counteraction to the increasing effect of concrete creep on edge stress is less evident comparing to that of adhesive creep in shear direction.

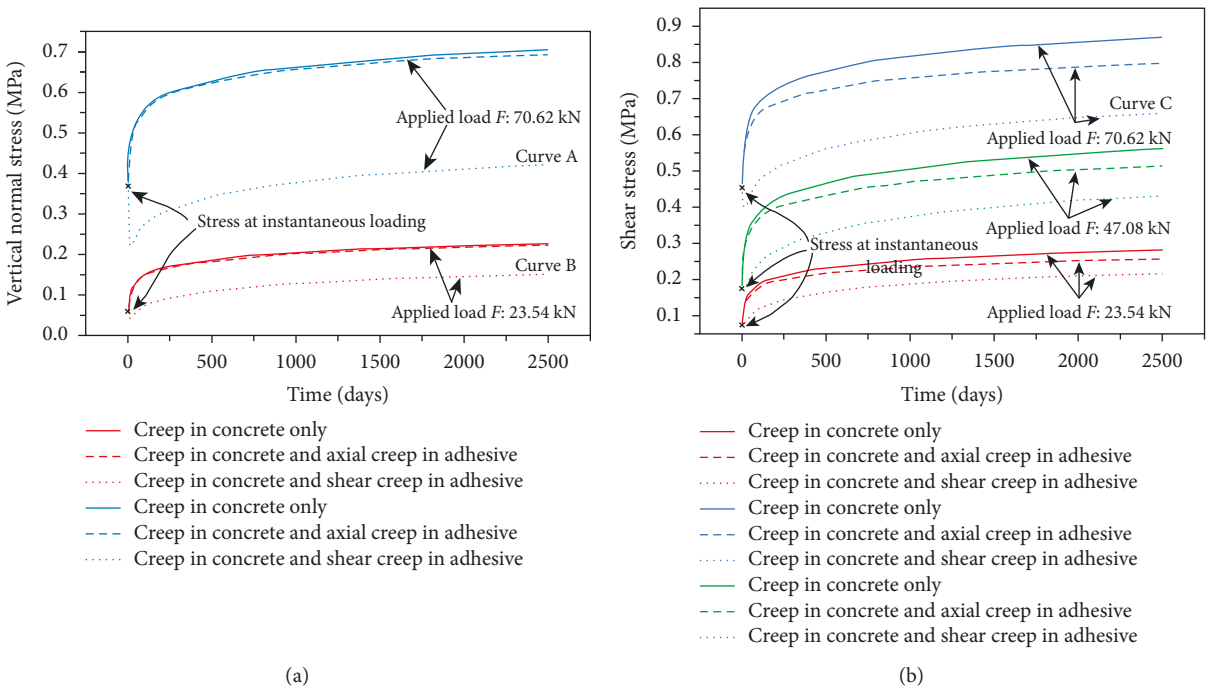

Figure 15: The combined effect of adhesive creep and concrete creep on the edge stresses. (a) Variation of vertical normal stress with time. (b) Variation of shear stress with time.

5. Conclusions

In this study, the challenges associated with the time-dependent analysis of RC members strengthened by bonding FRP externally have been discussed, and a finite element model has been developed. The recommended FE model simultaneously considers several aspects of the strengthened structures that the existing analytical methods do not take into account: the time-dependent characteristics of all components including the aging effect of concrete, the cracking behavior, and tension stiffening of concrete. These aspects have been considered through the constitutive laws of materials. User-defined subroutines embedded in the main FE program were used to model the time-dependent material properties. Unlike some existing analytical methods, specific simplifications were not included, which may further improve the general applicability of this FE approach.

The capability and accuracy of the proposed FE model were demonstrated through comparisons of its predictions with the results of test performed by the authors. Although, detailed changes of environmental conditions have not been considered and the average humidity during test was used to generally reflect the environmental effect, the FE-predicted results are in qualitative agreement with the experimental observations. Besides, test data in other research studies were also used to further verify the FE approach.

The analyses of interfacial stresses can be carried out through the same FE model, which only requires mesh refinement near the plate end, rather than to build a quite different analytical model from the beginning. The analyses show that concrete creep causes a significant increase in the shear and vertical normal stresses in the adhesive layer at the edges. This phenomenon may initiate debonding failure, which is of critical importance for the design of FRP-strengthened beams. Whereas, the viscoelastic adhesive may present a favorable effect on alleviating such problem, since it has been presented that the viscous flow of adhesive can relieve the edge stresses.

The FE model developed in this study may set a theoretical platform to better analyze the time-dependent characteristics of FRP-strengthened concrete structures. Further aspects of the structural behavior including effects of environment changes (e.g., variations of humidity and temperature), development of debonded regions, and creep rupture need to be further researched, which can be built on the findings and concepts of this study.

Data Availability

The data in Figures 3 and 6 used to support the findings of this study may be released upon application to the corresponding author (e-mail: jiangshiy@163.com). Previously reported data in Figure 9 were used to support this study and are available at doi: 10.1016/j.conbuildmat.2011.11.006 and doi: 10.1061/(ASCE1090-0268(2006)10:6(474)). These prior studies (and datasets) are cited at relevant places within the text as references [42, 43].

Conflicts of Interest

The authors declare that they have no conflicts of interest.

Acknowledgments

The authors are grateful for the financial support from the Chongqing Science and Technology Committee (Project nos: cstc2015shmszx30006 and cstc2011ab0043).

References

[1] S. Hong, "Effects of the amount and shape of carbon fiber-reinforced polymer strengthening elements on the ductile behavior of reinforced concrete beams," *Mechanics of Composite Materials*, vol. 50, no. 4, pp. 427–436, 2014.

[2] S. Hong, "Effect of intermediate crack debonding on the flexural strength of CFRP-strengthened RC beams," *Mechanics of Composite Materials*, vol. 50, no. 4, pp. 523–536, 2014.

[3] M. Rezazadeh, H. Ramezansefat, and J. Barros, "NSM CFRP prestressing techniques with strengthening potential for simultaneously enhancing load capacity and ductility performance," *Journal of Composites for Construction*, vol. 20, no. 5, article 04016029, 2016.

[4] S. H. Aboubakr, U. F. Kandil, and M. R. Taha, "Creep of epoxy-clay nanocomposite adhesive at the FRP interface: a multi-scale investigation," *International Journal of Adhesion and Adhesives*, vol. 54, pp. 1–12, 2014.

[5] Y. Jeong, J. Lee, and W. S. Kim, "Modeling and measurement of sustained loading and temperature-dependent deformation of carbon fiber-reinforced polymer bonded to concrete," *Materials*, vol. 8, no. 2, pp. 435–450, 2015.

[6] Y. Jeong, M. M. Lopez, and C. E. Bakis, "Effects of temperature and sustained loading on the mechanical response of CFRP bonded to concrete," *Construction and Building Materials*, vol. 124, pp. 442–452, 2016.

[7] I. Costa and J. Barros, "Tensile creep of a structural epoxy adhesive: experimental and analytical characterization," *International Journal of Adhesion and Adhesives*, vol. 59, pp. 115–124, 2015.

[8] J. Jeon, J. Kim, and A. Muliana, "Modeling time-dependent and inelastic response of fiber reinforced polymer composites," *Computational Materials Science*, vol. 70, pp. 37–50, 2013.

[9] A. Sorzia, "Modelling of creep and stress relaxation test of a polypropylene microfibre by using fraction-exponential kernel," *Modelling and Simulation in Engineering*, vol. 2016, Article ID 3823047, 7 pages, 2016.

[10] J. Tanks, K. Rader, S. Sharp, and T. Sakai, "Accelerated creep and creep-rupture testing of transverse unidirectional carbon/epoxy lamina based on the stepped isostress method," *Composite Structures*, vol. 159, pp. 455–462, 2017.

[11] S. Hong and S. K. Park, "Long-term behavior of fiber-reinforced-polymer-plated concrete beams under sustained loading: analytical and experimental study," *Composite Structures*, vol. 152, pp. 140–157, 2016.

[12] D. Trost, *Stress Relaxation of Concrete Structures and Relaxation Tests of Very Old Concrete*, Springer, Berlin, Germany, 1982.

[13] K. W. Nasser and A. M. Neville, "Creep of old concrete at normal and elevated temperature," *ACI Journal Proceedings*, vol. 64, no. 2, 1967.

[14] E. Hamed and M. A. Bradford, "Creep in concrete beams strengthened with composite materials," *European Journal of Mechanics-A/Solids*, vol. 29, no. 6, pp. 951–965, 2010.

[15] E. Hamed and M. A. Bradford, "Flexural time-dependent cracking and post-cracking behaviour of FRP strengthened concrete beams," *International Journal of Solids and Structures*, vol. 49, no. 13, pp. 1595–1607, 2012.

[16] A. R. Marí, E. Oller, J. M. Bairán, and N. Duarte, "Simplified method for the calculation of long-term deflections in FRP-strengthened reinforced concrete beams," *Composites Part B: Engineering*, vol. 45, no. 1, pp. 1368–1376, 2013.

[17] E. Oller and A. R. Marí, "Long-term bond stresses and debonding failure of FRP-strengthened RC cracked members," *Composites Part B: Engineering*, vol. 52, pp. 30–39, 2013.

[18] K. Hadjazi, Z. Sereir, and S. Amziane, "Creep response of intermediate flexural cracking behavior of reinforced concrete beam strengthened with an externally bonded FRP plate," *International Journal of Solids and Structures*, vol. 94-95, pp. 196–205, 2016.

[19] A. K. El-Sayed, R. A. Al-Zaid, A. I. Al-Negheimish, A. B. Shuraim, and A. M. Alhozaimy, "Long-term behavior of wide shallow RC beams strengthened with externally bonded CFRP plates," *Construction and Building Materials*, vol. 51, pp. 473–483, 2014.

[20] K. K. Choi, M. M. Reda Taha, M. J. Masia, P. L. Shrive, and N. G. Shrive, "Numerical investigation of creep effects on FRP-strengthened RC beams," *Journal of Composites for Construction*, vol. 14, no. 6, pp. 812–822, 2010.

[21] P. Meshgin, K. K. Choi, and M. M. R. Taha, "Experimental and analytical investigations of creep of epoxy adhesive at the concrete–FRP interfaces," *International Journal of Adhesion and Adhesives*, vol. 29, no. 1, pp. 56–66, 2009.

[22] S. Benyoucef, A. Tounsi, K. H. Benrahou, and E. A. Adda Bedia, "Time-dependent behavior of RC beams strengthened with externally bonded FRP plates: interfacial stresses analysis," *Mechanics of Time-Dependent Materials*, vol. 11, no. 3-4, pp. 231–248, 2007.

[23] C. Zhang and J. Wang, "Viscoelastic analysis of FRP strengthened reinforced concrete beams," *Composite Structures*, vol. 93, no. 12, pp. 3200–3208, 2011.

[24] J. G. Teng, J. W. Zhang, and S. T. Smith, "Interfacial stresses in reinforced concrete beams bonded with a soffit plate: a finite element study," *Construction and Building Materials*, vol. 16, no. 1, pp. 1–14, 2002.

[25] ABAQUS, *ABAQUS 6.12 User's Manual*, 2012.

[26] S. Jiang, W. Yao, J. Chen, and S. Tao, "Time dependent behavior of FRP-strengthened RC beams subjected to preload: experimental study and finite element modeling," *Composite Structures*, vol. 200, pp. 599–613, 2018.

[27] G. M. Chen, J. G. Teng, and J. F. Chen, "Finite element modeling of intermediate crack debonding in FRP-plated RC beams," *Journal of Composites for Construction*, vol. 15, no. 3, pp. 339–353, 2010.

[28] L. P. Saenz, "Discussion of equation for the stress-strain curve of concrete-by Desayi, P. and Krishan, S," *ACI Journal*, vol. 61, no. 9, pp. 1229–1235, 1964.

[29] D. A. Hordijk, "Local approach to fatigue of concrete," *Civil Engineering and Geosciences*, vol. 1, no. 4, pp. 442–448, 1991.

[30] CEB-FIP, *CEB-FIP Model Code 2010*, Ernst & Sohn Publishing House, Berlin, Germany, 2013.

[31] ACI Committee 318, *Building Code Requirements for Structural Concrete and Commentary*, American Concrete Institute, Farmington Hills, MI, USA, 2014.

[32] Z. P. Bazant and J. Planas, *Fracture and Size Effect in Concrete and Other Quasibrittle Materials*, CRC Press, Boca Raton, FL, USA, 1998.

[33] Z. P. Bažant and B. H. Oh, "Crack band theory for fracture of concrete," *Matériaux Et Construction*, vol. 16, no. 3, pp. 155–177, 1983.

[34] J. G. Rots, *Computational modeling of concrete fracture*, Ph.D. thesis, Delft University of Technology, Delft, The Netherlands, 1988.

[35] Y. Tao and J. F. Chen, "Concrete damage plasticity model for modeling FRP-to-concrete bond behavior," *Journal of Composites for Construction*, vol. 19, no. 1, article 04014026, 2015.

[36] Z. P. Bazant, "Prediction of creep effects using age-adjusted effective modulus method," *ACI Journal Proceedings*, vol. 69, no. 4, 1972.

[37] ACI Committee 209, *Prediction of Creep, Shrinkage, and Temperature Effects in Concrete Structures*, American Concrete Institute, Farmington Hills, MI, USA, 2002.

[38] C. W. Feng, C.-W. Keong, Y.-P. Hsueh, Y.-Y. Wang, and H.-J. Sue, "Modeling of long-term creep behavior of structural epoxy adhesives," *International Journal of Adhesion and Adhesives*, vol. 25, no. 5, pp. 427–436, 2005.

[39] W. N. Findley, J. S. Lai, K. Onaran, and R. M. Christensen, "Creep and relaxation of nonlinear viscoelastic materials," *Journal of Applied Mechanics*, vol. 44, no. 2, p. 364, 1977.

[40] Y. F. Wen, R. F. Gibson, and J. L. Sullivan, "Prediction of momentary transverse creep behavior of thermoplastic polymer matrix composites using micromechanical models," *Journal of Composite Materials*, vol. 31, no. 21, pp. 2124–2145, 1997.

[41] W. N. Findley, "Mechanism and mechanics of creep of plastics," *Society of Plastic Engineering Journal*, vol. 16, no. 1, pp. 57–65, 1960.

[42] H. R. Sobuz, E. Ahmed, N. Mohamed Sutan, N. M. Sadiqul Hasan, M. Alhaz Uddin, and M. Jahir Uddin, "Bending and time-dependent responses of RC beams strengthened with bonded carbon fiber composite laminates," *Construction and Building Materials*, vol. 29, pp. 597–611, 2012.

[43] K. H. Tan and M. K. Saha, "Long-term deflections of reinforced concrete beams externally bonded with FRP system," *Journal of Composites for Construction*, vol. 10, no. 6, pp. 474–482, 2006.

[44] O. Rabinovich and Y. Frostig, "Closed-form high-order analysis of RC beams strengthened with FRP strips," *Journal of Composites for Construction*, vol. 4, no. 2, pp. 65–74, 2000.

[45] E. Hamed and Z. T. Chang, "Effect of creep on the edge debonding failure of FRP strengthened RC beams–a theoretical and experimental study," *Composites Science and Technology*, vol. 74, pp. 186–193, 2013.